Batteries & Supercaps

Research Article
doi.org/10.1002/batt.202500064

Chemistry Europe
European Chemical Societies Publishing

www.batteries-supercaps.org

A Novel Non-Flammable Inorganic Liquid Electrolyte with Ultra-High Voltage Stability for Li-Ion Batteries

Vishwanathan Ramar, Christian Pszolla, Manuel Weinberger, Markus Borck, and Laurent Zinck*

The growing demand for high-performance energy storage has driven the search for advanced electrolytes in lithium-ion batteries (LIBs). Organic electrolytes (OEs) contribute to battery performance through their relatively good ionic conductivity and moderate temperature tolerance. However, their flammability and limited electrochemical stability, particularly at higher voltages pose significant safety risks and can reduce battery lifespan. We introduce a novel ultra-high-voltage (UHV), non-flammable inorganic liquid electrolyte based on a proprietary fluorinated salt in SO_2, stable to 5.2 V. It delivers high ionic conductivity (37.9 mS/cm at 25 °C; 21.1 mS/cm at −20 °C) and operates from −40 °C to 60 °C. By suppressing cathode oxygen release, it minimizes harmful side reactions, extending cell longevity. Testing with NMC811, LMR, and LMFP cathodes at 4.7 V yielded record specific capacities of 255, 299, and 158 mAh/g, respectively. Full-cells paired with graphite retained 90%, 81%, and 73% capacity after 1,200 cycles with ≈99.98% coulombic efficiency. In 21700 formats, the electrolyte enables 300 Wh/kg without adding silicon materials in the graphite anode. The thermal energy released during thermal runaway is reduced by 43% compared to OE. At −40 °C, cells maintained 83% of residual capacity. This technology offers improved safety, broad temperature tolerance, and exceptional electrochemical performance, offering a clear path to next-generation, sustainable LIBs.

1. Introduction

The world requires enormous amounts of sustainable energy in clean and renewable form for the energy transformation. The next 10 years will probably be the most innovative and productive era for mankind regarding energy storage technology development and we will realize a complete paradigm shift from our fossil fuel-based economy to an entirely renewable energy generation and storage economy. Since the first rechargeable Li-ion battery (LIB) was commercialized by Sony in 1991,[1,2] the constant innovations over three decades have resulted in a strong energy storage revolution from smart phones and laptops to the electrification of vehicles such as passenger cars, flying taxis, trucks, yachts, and planes. However, the increasing demand for novel electrochemical systems with higher energy density ($>300\ Wh\ kg^{-1}$) is essential to overcome the disadvantages of commercial LIBs for the electrification of vehicles. Improving the specific capacity of electrode active masses and/or working voltage is the most promising strategies to increase the specific energy of LIBs;[3–10] however, attention must be paid to safety at the same time. An ultra-high electrochemical stability of the electrolyte is key to enable higher electrochemical utilization of common cathode materials and to apply novel and more sustainable cathode chemistries to achieve specific energies beyond the state of the art. Besides high voltage stability, nonflammability, high conductivity, a wide range of operational temperatures, and compatibility with electrode materials are crucial for safe and robust battery operation.[7,8] A major practical bottleneck of current LIBs is the limited electrochemical stability (max. 4.2 V) and the flammability nature of organic electrolytes (OEs). These technical barriers, originating from the use of OEs, not only limit the full utilization of electrode materials and introduce safety concerns but also lead to slow electrochemical kinetics at subzero temperatures and reduced longevity.[7–21] In recent decades, fellow researchers have made great effort to improve electrochemical stability and the flame retardancy of OEs by using electrolyte additives,[22–24] ionic liquids as a cosolvent/solvent,[25–27] solid-state electrolytes,[28–33] and aqueous non-flammable electrolytes;[34,35] however, poor scalability and tremendous cost pose a huge challenge in realizing commercially applicable cells. Significant effort has been dedicated to developing solid electrolytes. However, they continue to face fundamental challenges, including lower ionic conductivity, dendrite formation within the solid electrolyte, interfacial stress, resistance, and surface reactions between the electrodes and the solid electrolyte. They also suffer from practicality issues such as 1) the need to wet the interfaces with liquid electrolyte and the application of external pressure in order to improve the rate performance, and 2) manufacturing difficulties and cost will increase due to the need of dual electrolytes to ensure the thermodynamic stability of both anode and cathode, which severely hinders the realization of solid-state batteries for commercial applications.[28–33] Furthermore, batteries with liquid electrolyte have advantages

V. Ramar, C. Pszolla, M. Weinberger, M. Borck, L. Zinck
Innolith Technology AG
Hirzbodenweg 95, 4052 Basel, Switzerland
E-mail: laurent.zinck@innolith.com

Supporting information for this article is available on the WWW under https://doi.org/10.1002/batt.202500064

over solid-state batteries in terms of design flexibility. Therefore, it is imperative to develop liquid electrolytes that meet the criteria of low cost, high voltage stability, nonflammability, a wide operational temperature range (−40 to 60 °C), and compatibility with most known electrode materials. In 1988, Foster et al.[36] demonstrated a liquid inorganic electrolyte (IE) consisting of $LiAlCl_4$ salt being solvated by gaseous SO_2,which shows high ionic conductivity of >100 mS cm^{-1} at RT, nonflammability, high Li^+ transference number, high dielectric constant due to the presence of SO_2 electric dipoles, and compatibility with lithium metal.[37–45] In a follow-up, researchers have reported the electrochemical performance of different cathode materials with IE such as $LiCoO_2$[37,43,44] and $LiFePO_4$ (LFP).[46,47] However, this electrolyte has a narrow voltage window of 3.2–4.0 V versus Li/Li^+ and is only suitable for LFP cathode materials to achieve chemically stable cycling.[37,44–46] Here, for the first time, a novel ultra-high voltage (UHV) non-flammable inorganic liquid electrolyte (I-State) for LIB materials was utilized to explore its compatibility with commercially applied and future cathode materials at high potentials ≫4.2 V. A wide variety of cathode materials were tested to show the superiority of the electrolyte. $LiFePO_4$||graphite cells are tested within a voltage window of 3.0–5.2 V, which shows no sign of side reactions. Half-cells of lithium nickel manganese cobalt oxides (NMC811), Li and Mn-rich layered oxide (LMR), and lithium iron manganese phosphate (LMFP) cathode materials were also tested, and they show the highest available specific capacities to date. The advantages of having UHV electrolyte in terms of additional capacity contribution for total capacity of the cell are discussed. The low-temperature performance of single-layer LMFP, NMC622, and NMC811||graphite 21700 cylindrical cells, with a specific energy of 300 Wh kg^{-1}, was evaluated down to −40 °C. This achievement is made possible by the exceptional low-temperature performance of the UHV electrolyte.

2. Results and Discussion

Increasing the specific energy (>350 Wh kg^{-1}) of electrochemical energy storage systems is essential to address the limitations of commercially available LIBs for vehicle electrification. Improving specific capacity and/or working voltage are the most promising strategies to achieve high specific energy LIBs. For instance, improving specific energy largely depends on the choice of cathode material. Layered oxide $LiNi_xCo_yMn_zO_2$ ($x = 1/3$, 0.5, 0.6, and 0.8) (NMC) is one of the most promising cathode materials due to its high specific capacity and voltage.[8,48,49] Although the theoretical capacity of NMC is 275 mAh g^{-1}, not all of this capacity can be accessed due to structural instabilities at higher voltages.[50–54] A higher specific capacity and energy can be achieved by increasing the charging cutoff voltage beyond the commonly applied 4.2 V.[50,51,55,56] However, charging a battery beyond 4.2 V can lead to electrolyte oxidation, the formation of a highly resistive CEI, and transition metal dissolution, resulting in fast capacity decay.[57–63] Due to the limited voltage stability (max. 4.3 V) of conventional OEs, Ni-rich NMC has gained significant interest recently, as more lithium can be extracted within a lower voltage window. However, the NMC cathode with higher Ni content experience larger unit cell volume changes during the de/intercalation reaction. This is related to the fact that the initial capacity increases with higher Ni content, which also leads to more severe capacity fading.[64–66] Noh et al.[64] reported initial specific capacities of 203 and 163 mAh g^{-1} for NMC811 and NMC111 versus Li/Li^+, respectively, with an upper voltage cutoff of 4.3 V at 0.1 C-rate. However, the capacity retention of NMC811 half-cells was only 70% compared to 92% for NMC111 after 100 cycles at 0.5 C-rate due to its significant volume change.[64] Apart from the limited electrochemical stability of commercial OEs, they also present other practical issues, such as flammability and sluggish electrochemical kinetics at subzero temperatures. For the very first time, an SO_2-based novel UHV non-flammable inorganic liquid electrolyte for LIB applications was utilized for LIB applications. This electrolyte possesses unique properties, resulting in excellent compatibility with various electrode materials and high voltage stability (5.2 V). Inductively coupled conductivity measurements showed that the maximum ionic conductivity of UHV electrolyte is 37.9 mS cm^{-1} at 25 °C. Temperature-dependent conductivity measurements with the optimum salt concentration clearly demonstrate a higher conductivity of 21.1 mS cm^{-1} even at −20 °C, which is significantly higher than that of OEs at RT (**Figure 1**a). The SO_2-based UHV electrolyte is not a supercooled

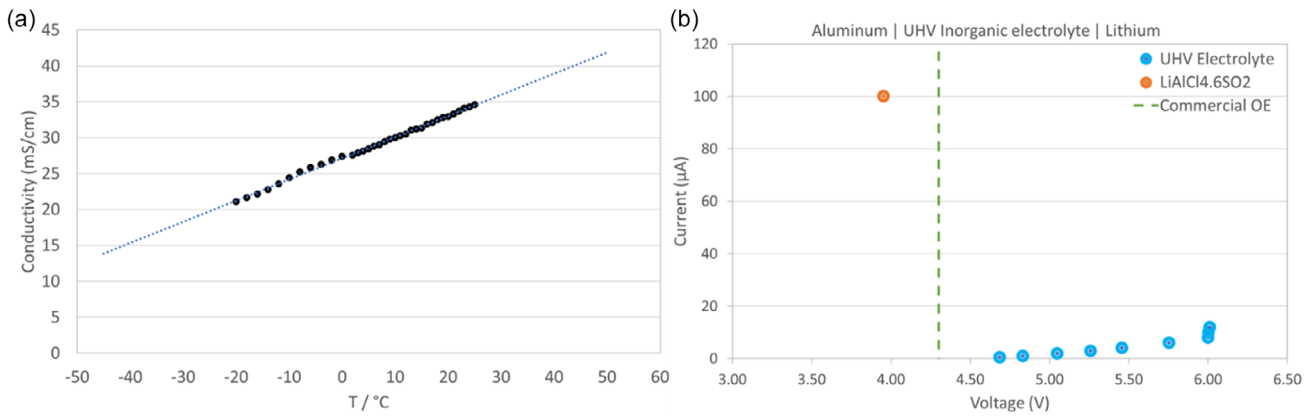

Figure 1. a) Temperature-dependent Ionic conductivity measurement of novel UHV liquid IE between −20 and 25 °C and b) electrochemical stability of UHV electrolyte compared with commercial OE and $LiAlCl_4{\cdot}6SO_2$ electrolyte with SO_2 as a solvent.

Research Article
doi.org/10.1002/batt.202500064
Chemistry Europe
European Chemical Societies Publishing

melt, unlike the $LiAlCl_4{\cdot}6SO_2$ electrolyte, meaning that a freezing point cannot be observed (Figure S1, Supporting Information). The curve shows a slightly different temperature rise behavior between −92 and −57 °C, attributed to the beginning and ending of a melting process of UHV electrolyte. The onset temperature of solidification at −57 °C significantly enhances the operation window of our electrolyte. This characteristic behavior is beneficial for subzero temperature operation of electrochemical cells down to at least −40 °C.

The electrochemical stability of the UHV electrolyte was measured using a two-electrode setup, with lithium metal as the negative electrode and Al-foil as the positive working electrode. The stability was measured in potentiostatic mode up to 6 V, revealing negligible corrosion current of only 1 and 2 μA at 5.2 and 5.3 V, respectively (Figure 1b). Above 5.3 V, a gradual increase in current up to 10 μA at 6.0 V was observed, which is significantly lower compared to the $LiAlCl_4{\cdot}6SO_2$ electrolyte, also shown in Figure 1b (100 μA at 3.95 V). The voltage stability of our novel UHV electrolyte (≈5.3 V vs Li/Li^+) is ≈1 V higher than that of commercially available OE (≈4.3 V vs Li/Li^+). Furthermore, it is well known that Phospho-Olivine structured $LiFePO_4$ (LFP) is a very stable cathode material compared to layered oxide (e.g., NMC). LFP does not undergo structural destruction during de/intercalation processes, exhibiting no structural change and oxygen release. It also has the advantage of a very flat working potential, making it an appropriate cathode material to test the electrochemical stability of electrolytes. LFP||graphite full-cells were tested with the UHV electrolyte up to 5.2 V (**Figure 2**a) showing no signs of side reactions. Figure 2b demonstrates stable energy efficiency and a columbic efficiency of 99.98%, consistent with the potentiostatic measurement results, which showed negligible current up to 5.3 V versus Li/Li^+ (Figure 1b).

A wide variety of cathode materials were tested to demonstrate the superiority of the UHV electrolyte properties. **Figure 3**a shows typical charge profiles of NMC811, LMR, and LMFP cathode materials up to 4.7 V. The half-cells of these cathode materials were tested with state-of-the-art (SOTA) electrode densities of 3.7, 3.0, 2.0 g cm^{-3}, respectively, and they exhibit very high

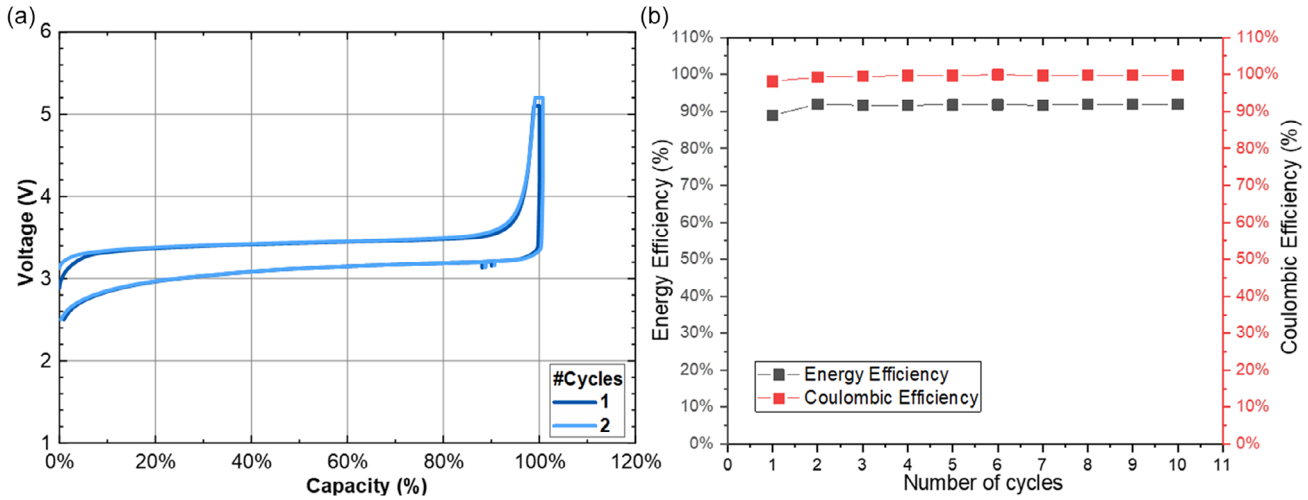

Figure 2. a) Charge–discharge curves of LFP cell at different upper voltage of 5.1 and 5.2 V, and b) Coulombic and energy efficiency at 5.2 V.

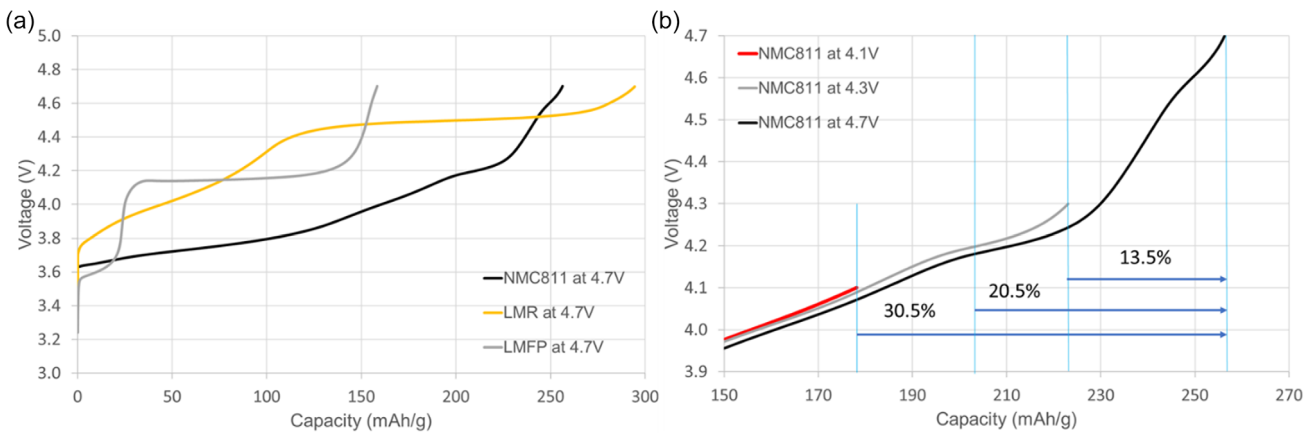

Figure 3. a) Typical first charge curves of NMC811, LMR, and LMFP cathode materials with UHV electrolyte at 4.7 V and b) extended charge curves of NMC811 material with UHV electrolyte at different upper voltage cut-off of 4.1, 4.3, and 4.7 V and percentage of capacity gain at 4.7 V from 4.1, 4.2, and 4.3 V.

available specific capacities of 255, 299, and 158 mAh g^{-1}, respectively, which are the highest values reported so far.[64,67–73] Figure 3b shows charge profiles of NMC811 with the UHV electrolyte at different charging cutoff voltages of 4.1, 4.3, and 4.7 V. These test results demonstrate a significant increase in first charge capacities of 30.5%, 20.5%, and 13.5% when NMC811 cells are charged to 4.7 V from 4.1, 4.2, and 4.3 V, respectively. This strategy allows us to extend the voltage limit of an NMC811–graphite full cell to well above 4.2 V. Due to the increased amount of usable lithium, less cathode material is needed to reach a certain capacity value. Indeed, we have previously demonstrated that 21700 cells with energy densities of 300 Wh kg^{-1} become feasible, even without the usage of silicon in the anode.

Figure 4a compares the performance of NMC811 half-cells using UHV electrolyte and a commercial ($LiPF_6$ in EC:EMC (3:7)) OE within the voltage cycling window of 3.0–4.7 V. The NMC811 electrode with the UHV electrolyte (IE) shows excellent discharge capacity retention of 95% after 50 cycles, compared to the OE counterpart, which retains only 68% of the initial capacity at 1 C. Additionally, UHV cells exhibit a 15% higher discharge capacity with a coulombic efficiency of 99.98%, whereas OE cells are limited to a coulombic efficiency of 99.2% (Figure 4b). The overall electrochemical performance of IE cells is superior in terms of discharge capacity, stability, and coulombic efficiency due to ultra-high electrochemical stability and higher conductivity of the IE (Figure 1 and 2). Jung et al.[74] reported that all NMC compositions (NMC111, NMC622, and NMC811) release oxygen at the state-of-charge (SoC) of ≈80–90%, with the onset potential for oxygen evolution at around 4.3 V versus Li/Li^+ (or 4.2 V vs graphite) for NMC811 and around 4.7 V versus Li/Li^+ (or 4.6 V vs graphite) for NMC111 and NMC622 materials.[54,74] The observed CO_2 and CO evolution are mainly due to the chemical reaction of released lattice oxygen from NMC with the OE.[54,74] However, NMC811 cells with the UHV electrolyte exhibit very stable performance even at 4.7 V versus Li/Li^+ as shown in Figure 4. We believe that oxygen release from the cathode surface is effectively suppressed in UHV cells. This is due to the intrinsically oversaturation of oxygen in the IE and the absence of detrimental reactions with the NMC811 cathode material. Therefore, the oxygen release and subsequent reactions with cell components, as described for OE when cycled at elevated potential,[74] do not occur with the IE. Figure S7, Supporting Information, illustrates the reaction scheme under high voltage charging conditions for IE versus OE. In traditional OE based on polycarbonate solvent and $LiPF_6$, high voltage charging conditions trigger a series of detrimental reactions. The oxygen released from the NMC811 cathode reacts with the electrolyte, leading to its decomposition. This process generates hydrogen fluoride (HF) and highly reactive nickel ions (Ni^{4+}). The highly corrosive HF passivates the current collector, impeding electron transfer, while the Ni^{4+} ions induce OE decomposition to form a resistive cathode electrolyte interphase (CEI). The cumulative effect of these reactions results in a battery cell with compromised stability, characterized by a low cycle life and premature failure (Figure 4). In contrast, the novel IE shows a significantly superior electrochemical stability. This inherent stability eliminates the decomposition pathways observed in OE. Additionally, the fluorinated conductive salt prevents the release of HF. Furthermore, the IE's oversaturation with oxygen inhibits the oxygen release from the cathode material, thereby preventing the NMC811 degradation. By avoiding these degradation mechanisms, the UHV IE supports a stable battery cell even when cycled up to 4.7 V versus Li/Li+.

According to the literature,[75] SO_2 is obtained by burning either elemental sulfur, various metal sulfides or organic sulfur compounds. The formation of SO_3 is not reported in the reaction of SO_2 with an excess of oxygen. It is challenging to obtain SO_3 from SO_2, as the process requires high temperatures of ≈450 °C and the presence of a catalyst.

The maximum energy released by the oxidation of SO_2 is negligible due to the reasons mentioned above (**Table 1**). The enthalpy calculation of the UHV proprietary salt is based on the values of bond strengths, ionization, and crystallization enthalpies of the salt, assuming a similar decomposition mechanism to $LiPF_6$ (Table S1, Supporting Information).[76] The decomposition temperature of the UHV proprietary salt (232 °C) is significantly higher than that of $LiPF_6$ (107 °C), indication better thermal stability (Table S2, Supporting Information).[77] These decomposition reactions of the salts are endothermic, and the heat absorbed can mitigate the thermal runaway (TR). The negative impact of decomposition products on TR is less likely with the

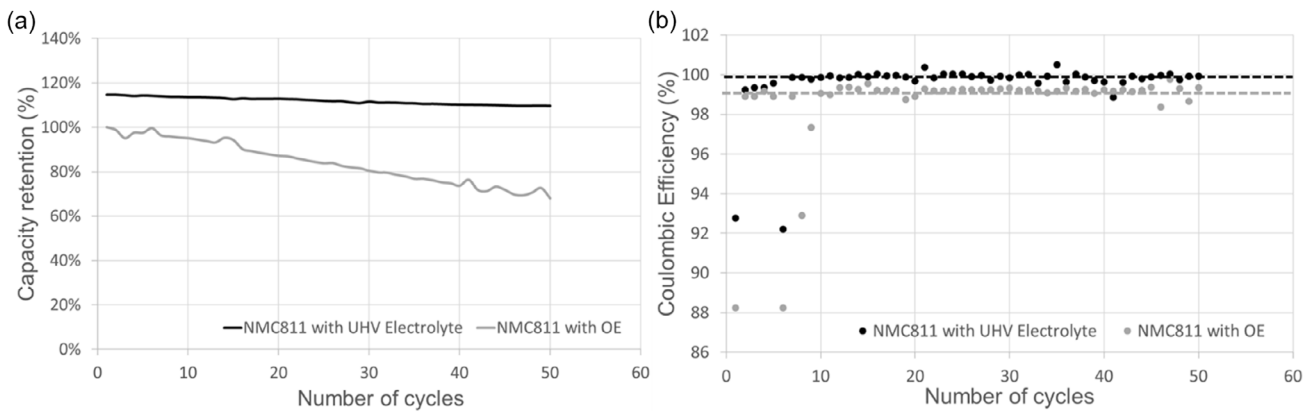

Figure 4. Performance comparison of NMC811 versus Li/Li^+ with UHV electrolyte and commercial OE at 1 C and 4.7 V: a) cycling stability and b) Coulombic efficiency.

Research Article
doi.org/10.1002/batt.202500064
Chemistry Europe
European Chemical Societies Publishing

Table 1. Specific energy of separator and electrolyte components.

Comparison of specific energies	I-State 21700 cell from Innolith		SOTA OE 21700 cell	
Component	Material	Energy [Wh]	Material	Energy [Wh]
Separator	PP [16 μm]	18.72	PP [16 μm]	18.72
Electrolyte				
Electrolyte	I-State	0.00	LP57	31.63
Total energy in 21700 cell				
Chemical energy	Combustible materials: separator + electrolyte	18.72		50.35
Electrical energy	Nominal voltage to fully charged state	20.00		18.00
Total	Chemical + electrical	38.72		68.35
Energy difference	43% less combustible energy/materials	57%		100%

UHV salt compared to $LiPF_6$. The type of organic solvents used with $LiPF_6$ salt also significantly affects the OE and overall battery performance.[78,79] Additionally, the decomposition temperature of the UHV salt exceeds the melting temperature of the separator and the electrolyte evaporation temperatures (130–140 °C).[80–83] The calculated total enthalpy value of the UHV salt is comparable to the total decomposition enthalpy of $LiPF_6$. However, its endothermic contribution to the cell's total enthalpy is negligible. Thus, the net energy released during the TR is almost negligible for UHV electrolyte compared to commercial OE (Table 1). Most importantly, the overall net heat released from UHV cells in the event of TR is 43% less than that of typical commercial OE cells (Table 1).

A differential capacity plot (d*Q*/d*V*) of NMC811 and NMC532 (Figure S2, Supporting Information) electrodes with the UHV electrolyte is depicted in **Figure 5**a. The two anodic peaks between 3.4 and 3.8 V are very similar for these two NMC compositions. The first peak originates from lithium intercalation into graphite, and the second peak corresponds to the phase transition from a hexagonal to a monoclinic (H1 → M) phase.[64,74,84–87] In the voltage region above 3.8 V, it is obvious that the d*Q*/d*V* for NMC811 cells is significantly different from that of the NMC532 cells. The NMC811||graphite cells exhibit an anodic features at ≈3.95 and 4.15 V, corresponding to the M → H2 and H2 → H3 phase transitions, respectively. These features are absent or broadened in NMC532 cells as reported for $LiNiO_2$[84–86] and Ni-rich NMC.[64,74,87] We did not observe peaks beyond the original lattice structural transition of NMC materials up to 4.6 V (graphite intercalation → H1 → M → H2 → H3) which might correspond to an oxygen redox feature witnessed in the literature for $Li_2Ru_{1-y}Sn_yO_3$[88] and Li_2IrO_3.[89–91] To explore the capacity contribution of each phase transition in NMC811-graphite cells at C/3, the differential capacity curve was integrated for each of the anodic peaks: 1) graphite intercalation peak at ≈3.45 V (peak 1), 2) H1-M peak at 3.65 V (peak 2), 3) M-H2 at 3.95 V (peak 3), and 4) H2–H3 at 4.15 V (peak 4). The percentage of integrated charge capacity for each phase transition with respect to the total available capacity (255 mAh g^{-1} in this case) is displayed in Figure 5a,b. The capacity contribution from the anodic peaks is ≈16%, 38%, 21%, and 25% for peaks 1, 2, 3, and 4, respectively, which are consistent with published ratios.[92] According to the literature, the electrochemical stability limit is 4.0 V for

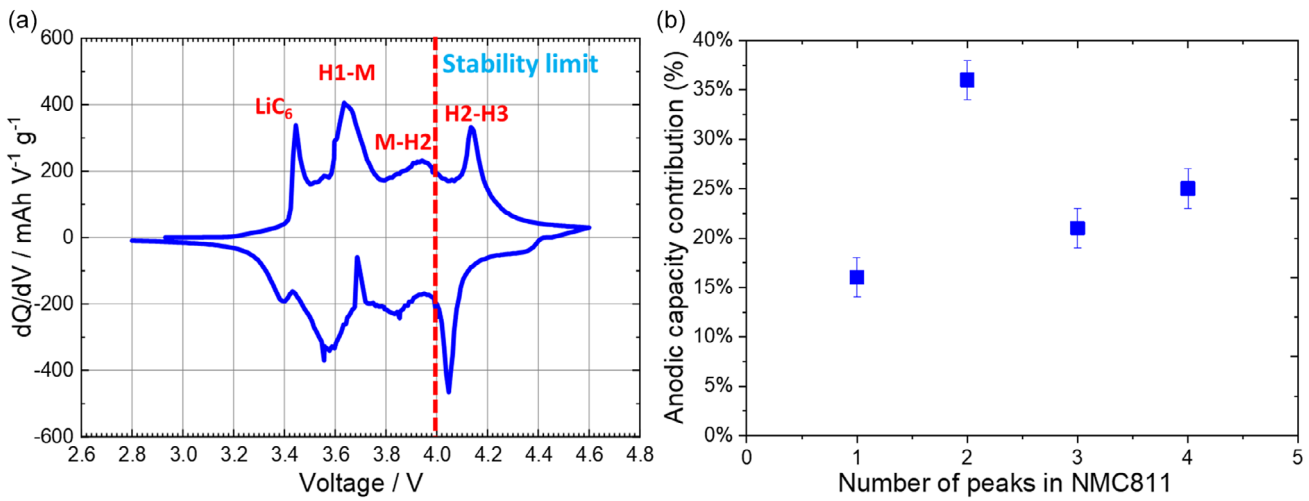

Figure 5. a) d*Q*/d*V* plot of NMC811||graphite cell charged to 4.6 V (red dotted line represents stability limit of 4.06 V for NMC811 materials in OE electrolyte as per literature[74]) and b) breakdown of capacity contribution of NMC811 versus graphite cell charged to 4.6 V with respect to total capacity; peak 1: first graphite intercalation stage, peak 2: H1-M, peak 3: M-H2, and peak 4: H2–H3.

Research Article
doi.org/10.1002/batt.202500064
Chemistry Europe
European Chemical Societies Publishing

NMC811||graphite cells cycled in OE. If the charge cutoff is limited to 4.0 V, a fourth peak contribution of ≈25% (64 mAh g^{-1}) cannot be explored, and only about 75% of the available capacity can be obtained. By extending the voltage limit to 4.6 V versus graphite using the UHV electrolyte (Figure 4), a gain of over 20% more capacity was achieved. This result is only possible due to the highly stable IE in combination with excellent compatibility with the electrode materials.

To demonstrate that the novel UHV technology can be charged quickly, charge rate tests were conducted with dense NMC811 and LMR electrodes versus graphite (NMC811||graphite and LMR||G) within a voltage window of 2.8–4.6 V (**Figure 6**a and Figure S5, Supporting Information). NMC811||graphite cells exhibited excellent charge capacities of 95%, 95%, 93%, 90%, 88%, 86%, and 83% of initial capacity (measured at C/10) at C/5, C/2, 1C, 2C, and 4C (15 min of charging), respectively, clearly outperforming the SOTA (Figure 6a). Similarly, the charge rate of LMR||G cells was explored up to 3 C. These cells showed very good charging capacities of 99%, 82%, 76%, 69%, and 67% of initial capacity (measured at C/15) at C/5, C/3, C/2, 1C, 2C, and 3C (20 min of charging), respectively (Figure 6a). All cells demonstrated impressive charge rate performances due to the stability and higher conductivity of the UHV electrolyte at RT. The cycle stability of the UHV electrolyte, when cycled to 4.6 V at RT, was investigated for LMFP, NMC811, and LMR cathode coupled with graphite anodes, as shown in Figure 6b and Figure S6, Supporting Information (NMC622, NMC532). Typical charge–discharge profiles of LMFP and LMR cathode materials are shown in Figure S3 and S4, Supporting Information. LMFP, NMC811, and LMR cycled versus graphite showed capacity retention of 90%, 83%, and 73% of the initial capacity (Figure 6b), respectively, after 1200 cycles with a coulombic efficiency of about 99.98% at C/3, clearly outperforming the competition.[64,67–73] Apart from high voltage stability and high ionic conductivity, it should be noted that the IE forms a highly stable solid electrolyte interface (SEI) on the graphite anode during prolonged cycling. This contrasts with LIBs cycled in OEs, where continuous electrolyte decomposition is common. Further studies on SEI formation on graphite surfaces in UHV electrolyte have been conducted and will be published at a later stage.

Subzero temperature performance was tested under isothermal conditions (**Figure 7 and 8**). The single-layer cells were cycled between 20 and −40 °C within the voltage window of 2.8–4.6 V at C/3. The NMC622||G cells showed 82%, 73%, and 61% of the initial

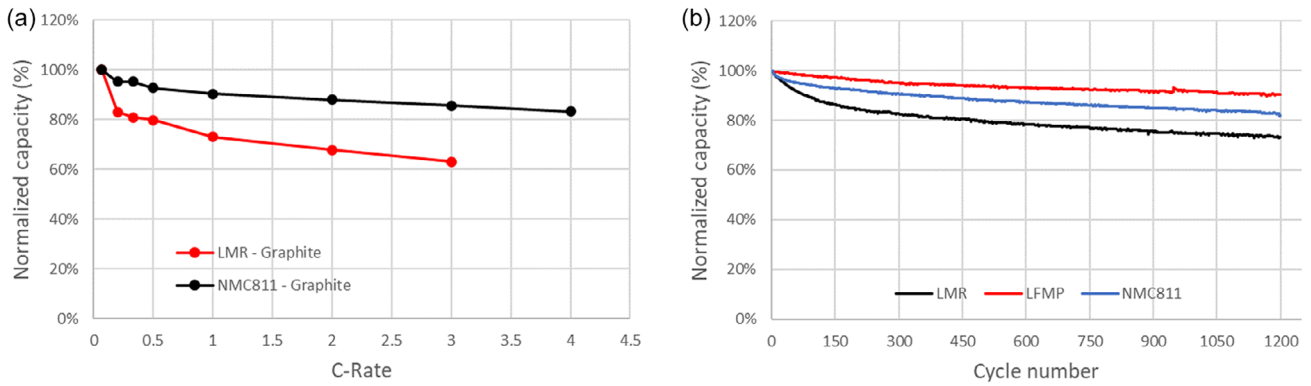

Figure 6. a) Charge rate test of NMC811 and LMR versus graphite cell at 0.1–4 C and b) long-term stability of NMC811, LMFP, and LMR cathode materials versus graphite anode material cycled within a voltage window of 2.8–4.6 V at C/3.

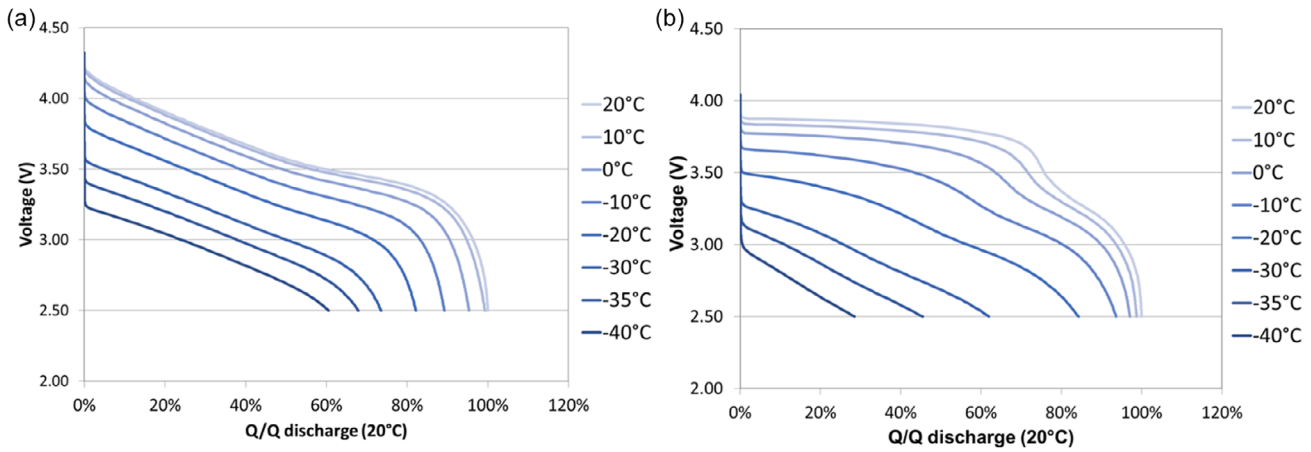

Figure 7. a) Extreme low-temperature performance of a single-layer prismatic cell cycled with UHV electrolyte. The cells are tested between 20 and −40 °C within a voltage window of 2.8–4.6 V at C/3: a) NMC622||graphite and b) LMFP||graphite cells.

Research Article
doi.org/10.1002/batt.202500064
Chemistry Europe
European Chemical Societies Publishing

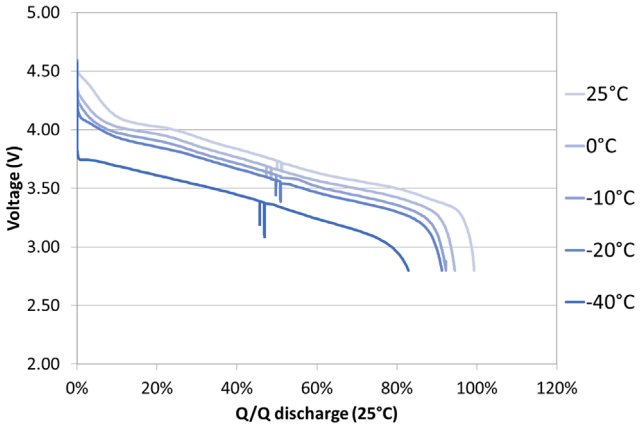

Figure 8. Extreme low-temperature performance of a high energy 21700 cylindrical cell (with an energy density of 300 Wh kg^{-1}) containing NMC811||graphite and filled with UHV electrolyte and tested between 25 and −40 °C within a voltage window of 2.8–4.6 V at C/3. The spikes at 50% SoC result from resistance testing with short pulses (1 ms and 5 s) with higher currents.

capacity (measured at 20 °C) at subzero temperatures of −20, −30, and −40 °C, respectively (Figure 7a). Similarly, single-layer LMFP||G cells showed 84% and 62% of initial capacity (20 °C) at deep temperatures of −20 and −30 °C, respectively (Figure 7b). The 21700 prototype cells with a specific energy of 300 Wh kg^{-1} were also tested under extreme subzero temperatures down to −40 °C (Figure 8). NMC811 and graphite electrodes were manufactured using commercially applied recipes and lab-scale equipment. The resulting 21700 cells were tested within the voltage cycling window of 2.8–4.6 V at C/3. For the first time, 21700 cylindrical cells delivered capacities of 95%, 92%, 91%, and 83% of initial capacity (measured at 25 °C) at subzero temperatures of 0, −10, −20, and −40 °C, respectively. These exceptional results were possible due to the high conductivity (21.1 mS cm^{-1} at −20 °C) and low melting point (−57 °C) of the UHV electrolyte.

3. Conclusions

A novel inorganic liquid electrolyte with UHV stability and nonflammability was developed for LIBs. It demonstrates high ionic conductivity (37.9 mS cm^{-1} at room temperature and 21.1 mS cm^{-1} at −20 °C), excellent thermal stability, and a wide operational temperature range (−40–60 °C). The net energy contribution from electrolyte during thermal runaway is negligible compared to commercial OEs. Most importantly, the overall net heat released from 21700 cylindrical cells with IE in the event of TR is 43% less than that of typical commercial OE cells. Various cathode materials were tested, showing the IE's superiority. $LiFePO_4$||graphite cells cycled up to 5.2 V exhibited no side reactions and a coulombic efficiency of 99.98%. Half-cells of NMC811, LMR, and LMFP with commercially viable electrode densities achieved extraordinary capacities of 255, 299, and 158 mAh g^{-1} at 4.7 V, the highest reported to date. The cells gained over 20% additional capacity compared to OE cells, extending the voltage limit of NMC811–graphite cells beyond 4.2 V. With more available lithium, less cathode material is required to achieve a specific capacity. We have demonstrated that 21700 cells with energy densities of 300 Wh kg^{-1} are feasible without silicon in the anode. Charge rate tests of NMC811||graphite cells showed 84% capacity retention after 15 min of charging. Cells with LMFP, NMC811, and LMR versus graphite retained 90%, 83%, and 73% of initial capacity, respectively, after 1200 cycles with a Coulombic efficiency of ≈99.98% at C/3. NMC811||graphite 21700 cells show discharged capacities of 95%, 92%, 91%, and 83% at subzero temperatures of 0, −10, −20, and −40 °C, respectively. The novel IE offers an outstanding alternative for LIBs, widening the voltage stability window, providing exceptional subzero temperature performance, increasing safety and suppressing oxygen reactivity and passivation reactions at the cathode surface. Future research should focus on optimizing IE composition and exploring new cathode materials to further enhance battery performance. Additionally, scaling up production and integrating this technology into commercial applications will be crucial for advancing energy storage solutions.

4. Experimental Section

Electrolyte Preparation

A proprietary fluorinated conductive salt with a purity of 98% was synthesized in-house. This conductive salt was mixed with liquid SO_2 to form a transparent liquid electrolyte. The concentration of SO_2 was determined by measuring the weight of the glass electrolyte vessel before and after the introduction of the liquid/gaseous SO_2.[37,44,45]

Electrolyte Characterization

The ionic conductivity of the high voltage non-flammable inorganic liquid electrolyte (SO_2 solvated proprietary fluorinated conductive salt) was measured using inductive coupled conductivity measurement as a function of temperature and SO_2 concentration. The conductivity measurement was carried out within a temperature range of −20 to 25 °C. After determining the maximum conductivity at the optimum molar concentration, the solution was placed in the conductivity measuring apparatus. The solution was then cooled down to −20 °C with the help of a cold mixture and the conductivity values were recorded during the warming process. The electrolyte's density (1.6 g cm^{-3}) was measured using a density hydrometer with an integrated thermometer. The experimental apparatus was immersed in a 0.5 l Dewar flask and positioned such that the pressure glass flask was completely covered with liquid nitrogen. The entire thawing process (evaporation of the liquid nitrogen) was recorded using a data logger. The thermocouple's mini plug was connected to the data logger's mini adapter, and the logging program was initiated.

Electrode Preparation

All chemicals were sourced from established chemical manufacturers. Cathode and anode materials were purchased from common mass battery material producers. Cathode electrodes were prepared using either NMC, LMR, or LMFP as active materials (CAM), along with a conductive additive (CB, Alfa Aesar) and binder (PVDF, Solvay), with *N*-methyl pyrrolidone (NMP) as solvent and dispersing medium. The final electrode composition for all cathodes was set to 96.5:1.5:2 (wt%) for CAM:CB:PVDF. The viscous slurry was coated

onto aluminum foil under ambient climate conditions, followed by evaporation of the NMP solvent through overnight drying at 80 °C under vacuum. Typical dry electrode loadings were measured as follows: 16.3 mg cm^{-2} for NMC, 21.4 mg cm^{-2} for LMR, and 16.7 mg cm^{-2} for LFMP. All electrodes were calendared using a twin roller (Eirich twin roller) to achieve the desired electrode densities: 3.7 g cm^{-3} for NMC, 3.0 g cm^{-3} for LMR, and 2.0 g cm^{-3} for LMFP.

Anode electrodes were prepared using graphite as the active material (AAM), with carboxymethyl cellulose and styrene-butadiene rubber binders (CMC + SBR, 50:50 wt% mixture), and water as the solvent. The electrode composition was set to 96:4 (wt%) for AAM:CMC + SBR. The viscous slurry was coated onto Cu-foil under ambient climate conditions, and the solvent was evaporated by drying the electrodes at 80 °C overnight under vacuum. The electrodes were calendared using a twin roller to achieve the desired density of 1.7 g cm^{-3}.

Cell Assembly

Half-cells: Three-electrode cells were assembled with either NMC, LMR or LMFP as the working electrode, with Li-metal as counter and reference electrodes. A nonwoven glass separator was utilized, and the IE was filled into the cell in the desired amount.

Full-cells: Prismatic cells were assembled by stacking either NMC, LMR, or LMFP as cathodes with graphite anodes, using either a nonwoven glass separator or a 16 μm polypropylene (PP) separator. The assembled stack was placed in a stainless-steel housing, insulated to protect it from the housing, and subsequently sealed using laser welding. The cells were dried overnight at 80 °C under vacuum. The desired amount of IE was then introduced into the cells through a filling tube attached to the cell lid, which was subsequently sealed by laser welding. NMC811||graphite 21700 cylindrical cells were manufactured using a 16 μm PP separator on a semiautomated pilot line. The desired amount of IE was introduced into the cells using proprietary filling equipment specially designed for 21700 cells.

Electrochemical Characterization

NMC/LMR/LMFP versus Li/Li^+ half-cells were cycled in constant current (CC) mode for both, charge and discharging processes within a voltage window of 3.0–4.7 V at RT. NMC/LMR/LMFP versus graphite prismatic cells were evaluated using CC cycling within a voltage window of 2.8–4.6 V. NMC811||graphite 21700 cylindrical cells, with a specific energy of 300 Wh kg^{-1}, were tested using CC-constant voltage (CV) cycling within a voltage window of 2.8–4.6 V, utilizing BaSyTec battery tester. Capacity values were calculated based on the weight of the active material in the electrodes. All electrochemical tests were conducted using several batches of cells, with eight cells in each batch. For simplicity, we present in our work average values for the eight cells. The electrochemical stability of the electrolyte was evaluated through potentiostatic testing using Li||UHV electrolyte||Al-foil cells. Potential levels were set to 4.6, 4.8, 5.0, 5.2, 5.4, 5.6, 5.8, and 6.0 V, with each potential maintained for 5 h and a current limited to 0.13 mA (0.1 mA cm^{-2}).

Acknowledgements

The authors thank all the Innolith supporting team of electrode and electrolyte production, cell production, filling, and testing.

Conflict of Interest

The authors declare no conflict of interest.

Author Contributions

Laurent Zinck: conceptualization (lead); funding acquisition (lead); investigation (lead); supervision (lead); validation (lead); writing—original draft (equal); writing—review and editing (lead). **Vishwanathan Ramar**: conceptualization (supporting); formal analysis (lead); investigation (lead); project administration (lead); writing—original draft (lead). **Christian Pszolla**: conceptualization (equal); formal analysis (lead); investigation (supporting); project administration (equal); writing—original draft (equal). **Manuel Weinberger**: conceptualization (supporting); methodology (lead); supervision (equal); visualization (lead); writing—original draft (equal). **Markus Borck**: funding acquisition (supporting); validation (equal); visualization (equal); writing—review and editing (supporting).

Data Availability Statement

The data that support the findings of this study are available from the corresponding author upon reasonable request.

Keywords: electrochemical storage · high voltage · high voltage cathode materials · lithium-ion chemistry · non-flammable liquid inorganic electrolytes

[1] www.nobelprize.org/prizes/chemistry/2019, *The Nobel Prize in Chemistry* **2019**.
[2] A. Yoshino, K. Sanechika, T. Nakajima, Patent, US4668595A - 1986.
[3] V. Ramar, P. Balaya, *J. Power Sources* **2016**, *306*, 552.
[4] V. Ramar, K. Saravanan, S. R. Gajjela, S. Hariharan, P. Balaya, *Electrochim. Acta* **2013**, *105*, 496.
[5] K. Saravanan, V. Ramar, P. Balaya, J. J. Vittal, *J. Mater. Chem.* **2011**, *21*, 14925.
[6] V. Ramar, P. Balaya, *Phys. Chem. Chem. Phys.* **2013**, *15*, 17240.
[7] J. B. Goodenough, *Nat. Electron.* **2018**, *1*, 204.
[8] M. S. Whittingham, *Chem. Rev.* **2004**, *104*, 4271.
[9] J.-M. Tarascon, M. Armand, *Nature* **2001**, *414*, 359.
[10] M. Armand, J.-M. Tarascon, *Nature* **2008**, *451*, 652.
[11] J. B. Goodenough, Y. Kim, *Chem. Mater.* **2010**, *22*, 587.
[12] P. G. Bruce, B. Scrosati, J.-M. Tarascon, *Angew. Chem. Int. Ed.* **2008**, *47*, 2930.
[13] B. Dunn, H. Kamath, J.-M. Tarascon, *Science* **2011**, *334*, 928.
[14] D. Aurbach, Y. Ein-Ely, A. Zaban, *J. Electrochem. Soc.* **1994**, *141*, L1.
[15] J. W. Choi, D. Aurbach, *Nat. Rev. Mater.* **2016**, *1*, 1.
[16] E. M. Erickson, E. Markevich, G. Salitra, D. Sharon, D. Hirshberg, E. de la Llave, I. Shterenberg, A. Rosenman, A. Frimer, D. Aurbach, *J. Electrochem. Soc.* **2017**, *164*, X5.
[17] U.-H. Kim, D.-W. Jun, K.-J. Park, Q. Zhang, P. Kaghazchi, D. Aurbach, D. T. Major, G. Goobes, M. Dixit, N. Leifer, C. M. Wang, P. Yan, D. Ahn, K.-H. Kim, C. S. Yoon, Y.-K. Sun, *Energy Environ. Sci.* **2018**, *11*, 1271.
[18] E. Markevich, G. Salitra, P. Hartmann, J. Kulisch, D. Aurbach, K.-J. Park, C. S. Yoon, Y.-K. Sun, *J. Electrochem. Soc.* **2019**, *166*, A5265.
[19] S. Hess, M. Wohlfahrt-Mehrens, M. Wachtler, *J. Electrochem. Soc.* **2015**, *162*, A3084.
[20] M. C. Smart, B. V. Ratnakumar, S. Surampudi, Y. Wang, X. Zhang, S. G. Greenbaum, A. Hightower, C. C. Ahn, B. Fultz, *J. Electrochem. Soc.* **1999**, *146*, 3963.
[21] M. C. Smart, B. V. Ratnakumar, S. Surampudi, *J. Electrochem. Soc.* **1999**, *146*, 486.
[22] K. Xu, M. S. Ding, S. Zhang, J. L. Allen, T. Richard Jow, *J. Electrochem. Soc.* **2002**, *149*, A622.
[23] X. Xia, P. Ping, J. R. Dahn, *J. Electrochem. Soc.* **2012**, *159*, A1834.
[24] Y. Liu, S. Fang, D. Luo, L. Yang, S. Hirano, *J. Electrochem. Soc.* **2016**, *163*, A1951.
[25] N. Salem, Y. Abu-Lebdeh, *J. Electrochem. Soc.* **2014**, *161*, A1593.

[26] N. Salem, S. Zavorine, D. Nucciarone, K. Whitbread, M. Moser, Y. Abu-Lebdeh, *J. Electrochem. Soc.* **2017**, *164*, H5202.
[27] R. Mantz, H. De Long, L. Haverhals, P. Trulove, *J. Electrochem. Soc.* **2017**, *164*, Y9.
[28] K. Kerman, A. Luntz, V. Viswanathan, Y.-M. Chiang, Z. Chen, *J. Electrochem. Soc.* **2017**, *164*, A1731.
[29] K. C. Santosh, R. C. Longo, K. Xiong, K. Cho, *J. Electrochem. Soc.* **2014**, *161*, F3104.
[30] R. Raj, J. Wolfenstine, *J. Power Sources* **2017**, *343*, 119.
[31] J. A. Lewis, J. Tippens, F. Javier Quintero Cortes, M. T. McDowell, *TRECHEM* **2019**, *1*, 845.
[32] C. Wang, K. Fu, S. P. Kammampata, D. W. McOwen, A. J. Samson, L. Zhang, G. T. Hitz, A. M. Nolan, E. D. Wachsman, Y. Mo, V. Thangadurai, L. Hu, *Chem. Rev.* **2020**, *120*, 4257.
[33] V. Thangadurai, H. Kaack, W. J. F. Weppner, *J. Am. Ceram. Soc.* **2003**, *86*, 437.
[34] L. Suo, Y.-S. Hu, H. Li, M. Armand, L. Chen, *Nat. Commun.* **2013**, *4*, 1.
[35] L. Suo, O. Borodin, T. Gao, M. Olguin, J. Ho, X. Fan, C. Luo, C. Wang, K. Xu, *Science* **2015**, *350*, 938.
[36] D. L. Foster, H. C. Kuo, C. R. Schlaikjer, A. N. Dey, *J. Electrochem. Soc.* **1988**, *135*, 2682.
[37] L. Zinck, M. Borck, C. Ripp, G. Hambitzer, *J. Appl. Electrochem.* **2006**, *36*, 1291.
[38] G. T.-K. Fey, W.-K. Liu, Y.-C. Chang, *J. Power Sources* **2001**, *97–98*, 602.
[39] N. Grundish, C. Amos, J. B. Goodenough, *J. Electrochem. Soc.* **2018**, *165*, A1694.
[40] A. Kim, H. Jung, J. Song, H. J. Kim, G. Jeong, H. Kim, *ACS Appl. Mater. Interfaces* **2019**, *11*, 9.
[41] J. Song, J. Chun, A. Kim, H. Jung, H. J. Kim, Y.-J. Kim, G. Jeong, H. Kim, *ACS Appl. Mater. Interfaces* **2018**, *10*, 34699.
[42] R. Hartl, M. Fleischmann, R. Gschwind, M. Winter, H. Gores, *Energies* **2013**, *6*, 4448.
[43] C. Wan Park, S. M. Oh, *J. Power Sources* **1997**, *68*, 338.
[44] C. Ripp, G. Hambitzer, L. Zinck, M. Borck, *Encyclopedia of Electrochemical Power Sources* (Eds: J. Garche, C. K. Dyer), Elsevier, Amsterdam, Oxford **2009**, p. 383.
[45] V. Ramar, C. Pszolla, M. Rapp, M. Borck, L. Zinck, *J. Electrochem. Soc.* **2020**, *167*, 70521.
[46] N. Grundish, C. Amos, J. B. Goodenough, *J. Electrochem. Soc.* **2018**, *165*, A1694.
[47] T. Gao, B. Wang, L. Wang, G. Liu, F. Wang, H. Luo, D. Wang, *Electrochim. Acta* **2018**, *286*, 77.
[48] I. Belharouak, Y.-K. Sun, J. Liu, K. Amine, *J. Power Sources* **2003**, *123*, 247.
[49] J. Choi, A. Manthiram, *J. Electrochem. Soc.* **2005**, *152*, A1714.
[50] S.-K. Jung, H. Gwon, J. Hong, K.-Y. Park, D.-H. Seo, H. Kim, J. Hyun, W. Yang, K. Kang, *Adv. Energy Mater.* **2014**, *4*, 1300787.
[51] H. Gabrisch, T. Yi, R. Yazami, *Electrochem. Solid-State Lett.* **2008**, *11*, A119.
[52] S.-M. Bak, E. Hu, Y. Zhou, X. Yu, S. D. Senanayake, S.-J. Cho, K.-B. Kim, K. Y. Chung, X.-Q. Yang, K.-W. Nam, *ACS Appl. Mater. Interfaces* **2014**, *6*, 22594.
[53] C. Xu, K. Märker, J. Lee, A. Mahadevegowda, P. J. Reeves, S. J. Day, M. F. Groh, S. P. Emge, C. Ducati, B. Layla Mehdi, C. C. Tang, C. P. Grey, *Nat. Mater.* **2021**, *20*, 84.
[54] D. Streich, C. Erk, A. Guéguen, P. Müller, F.-F. Chesneau, E. J. Berg, *J. Phys. Chem. C* **2017**, *121*, 13481.
[55] N. Yabuuchi, Y. Makimura, T. Ohzuku, *J. Electrochem. Soc.* **2007**, *154*, A314.
[56] M. G. Kim, H. J. Shin, J.-H. Kim, S.-H. Park, Y.-K. Sun, *J. Electrochem. Soc.* **2005**, *152*, A1320.
[57] I. Buchberger, S. Seidlmayer, A. Pokharel, M. Piana, J. Hattendorff, P. Kudejova, R. Gilles, H. A. Gasteiger, *J. Electrochem. Soc.* **2015**, *162*, A2737.
[58] M. Metzger, B. Strehle, S. Solchenbach, H. A. Gasteiger, *J. Electrochem. Soc.* **2016**, *163*, A798.
[59] D. R. Gallus, R. Schmitz, R. Wagner, B. Hoffmann, S. Nowak, I. Cekic-Laskovic, R. W. Schmitz, M. Winter, *Electrochim. Acta* **2014**, *134*, 393.
[60] H. Zheng, Q. Sun, G. Liu, X. Song, V. S. Battaglia, *J. Power Sources* **2012**, *207*, 134.
[61] Y.-C. Lu, A. N. Mansour, N. Yabuuchi, Y. Shao-Horn, *Chem. Mater.* **2009**, *21*, 4408.
[62] A. M. Andersson, D. P. Abraham, R. Haasch, S. MacLaren, J. Liu, K. Amine, *J. Electrochem. Soc.* **2002**, *149*, A1358.
[63] J. Wandt, A. Freiberg, R. Thomas, Y. Gorlin, A. Siebel, R. Jung, H. A. Gasteiger, M. Tromp, *J. Mater. Chem. A* **2016**, *4*, 18300.
[64] H.-J. Noh, S. Youn, C. S. Yoon, Y.-K. Sun, *J. Power Sources* **2013**, *233*, 121.
[65] W. Liu, P. Oh, X. Liu, M.-J. Lee, W. Cho, S. Chae, Y. Kim, J. Cho, *Angew. Chem. Int. Ed.* **2015**, *54*, 4440.
[66] J. Zheng, W. H. Kan, A. Manthiram, *ACS Appl. Mater. Interfaces* **2015**, *7*, 6926.
[67] F. Wu, S. Fang, M. Kuenzel, A. Mullaliu, J.-K. Kim, X. Gao, T. Diemant, G.-T. Kim, S. Passerini, *Joule* **2021**, *5*, 2177.
[68] Z. Yu, H. Wang, X. Kong, W. Huang, Y. Tsao, D. G. Mackanic, K. Wang, X. Wang, W. Huang, S. Choudhury, Y. Zheng, C. V. Amanchukwu, S. T. Hung, Y. Ma, E. G. Lomeli, J. Qin, Y. Cui, Z. Bao, *Nat. Energy* **2020**, *5*, 526.
[69] Q. Zhao, S. Stalin, L. A. Archer, *Joule* **2021**, *5*, 1119.
[70] F. Li, J. He, J. Liu, M. Wu, Y. Hou, H. Wang, S. Qi, Q. Liu, J. Hu, J. Ma, *Angew. Chem. Int. Ed.* **2021**, *60*, 6600.
[71] X. Fan, X. Ji, F. Han, J. Yue, J. Chen, L. Chen, T. Deng, J. Jiang, C. Wang, *Sci. Adv.* **2018**, *4*, eaau9245.
[72] P. Xiao, Y. Zhao, Z. Piao, B. Li, G. Zhou, H.-M. Cheng, *Energy Environ. Sci.* **2022**, *15*, 2435.
[73] S. Tan, Z. Shadike, J. Li, X. Wang, Y. Yang, R. Lin, A. Cresce, J. Hu, A. Hunt, I. Waluyo, L. Ma, F. Monaco, P. Cloetens, J. Xiao, Y. Liu, X.-Q. Yang, K. Xu, E. Hu, *Nat. Energy* **2022**, *7*, 484.
[74] M. M. Roland Jung, F. Maglia, C. Stinner, H. A. Gasteiger, *J. Electrochem. Soc.* **2017**, *164*, A1361.
[75] *A. F. Holleman, E. Wiberg, Lehrbuch der anorganischen Chemie*, Walter de Gruyter, Berlin **2007**.
[76] J. Y. Han, S. Jung, *Batteries* **2022**, *8*, 61.
[77] K. S. Gavritchev, G. A. Sharpataya, A. A. Smagin, E. N. Malyi, V. A. Matyukha, *J. Therm. Anal. Calorim.* **2003**, *73*, 71.
[78] B. S. Parimalam, B. L. Lucht, *J. Electrochem. Soc.* **2018**, *165*, A251.
[79] T. Teufl, D. Pritzl, S. Solchenbach, H. A. Gasteiger, M. Mendez, *Meet. Abstr.* **2018**, *MA2018-02*, 456.
[80] R. Spotnitz, J. Franklin, *J. Power Sources* **2003**, *113*, 81.
[81] D. P. Abraham, E. P. Roth, R. Kostecki, K. McCarthy, S. MacLaren, D. H. Doughty, *J. Power Sources* **2006**, *161*, 648.
[82] B. Manikandan, V. Ramar, C. Yap, P. Balaya, *J. Power Sources* **2017**, *361*, 300.
[83] M. Balasundaram, V. Ramar, C. Yap, L. Li, A. A. O. Tay, P. Balaya, *J. Power Sources* **2016**, *328*, 413.
[84] H. Arai, S. Okada, H. Ohtsuka, M. Ichimura, J. Yamaki, *Solid State Ionics* **1995**, *80*, 261.
[85] W. Li, J. N. Reimers, J. R. Dahn, *Solid State Ionics* **1993**, *67*, 123.
[86] J. P. Peres, F. Weill, C. Delmas, *Solid State Ionics* **1999**, *116*, 19.
[87] S.-U. Woo, C. S. Yoon, K. Amine, I. Belharouak, Y.-K. Sun, *J. Electrochem. Soc.* **2007**, *154*, A1005.
[88] M. Sathiya, G. Rousse, K. Ramesha, C. P. Laisa, H. Vezin, M. T. Sougrati, M.-L. Doublet, D. Foix, D. Gonbeau, W. Walker, A. S. Prakash, M. Ben Hassine, L. Dupont, J.-M. Tarascon, *Nat. Mater.* **2013**, *12*, 827.
[89] E. McCalla, A. M. Abakumov, M. Saubanère, D. Foix, E. J. Berg, G. Rousse, M.-L. Doublet, D. Gonbeau, P. Novák, G. van Tendeloo, R. Dominko, J.-M. Tarascon, *Science* **2015**, *350*, 1516.
[90] D.-H. Seo, J. Lee, A. Urban, R. Malik, S. Kang, G. Ceder, *Nature Chem.* **2016**, *8*, 692.
[91] M. Saubanère, E. McCalla, J.-M. Tarascon, M.-L. Doublet, *Energy Environ. Sci.* **2016**, *9*, 984.
[92] T. M. M. Heenan, A. Jnawali, M. D. R. Kok, T. G. Tranter, C. Tan, A. Dimitrijevic, R. Jervis, D. J. L. Brett, P. R. Shearing, *J. Electrochem. Soc.* **2020**, *167*, 140530.

Manuscript received: January 28, 2025
Revised manuscript received: April 4, 2025
Version of record online: